Zero electron kinetic energy spectroscopy of the $XeCl^-$ anion

Thomas Lenzer,[a] Ivan Yourshaw, Michael R. Furlanetto, Nicholas L. Pivonka, and Daniel M. Neumark[b]
Department of Chemistry, University of California, Berkeley, California 94720, and Chemical Sciences Division, Lawrence Berkeley National Laboratory, Berkeley, California 94720

(Received 9 November 2001; accepted 21 December 2001)

Zero electron kinetic energy spectroscopy has been used to study the $XeCl^-$ anion and the $X1/2$ electronic state of neutral XeCl. The spectrum is vibrationally resolved, yielding anion and neutral vibrational frequencies. With the aid of earlier scattering measurements for the neutral state we construct a Morse–Morse-switching–van der Waals model potential function for the anion from our spectroscopic data, for which $R_m = 3.57 \pm 0.03$ Å and $\epsilon = 145.8 \pm 0.7$ meV. This represents the first accurate experimental potential for the $XeCl^-$ anion. © *2002 American Institute of Physics.* [DOI: 10.1063/1.1450551]

I. INTRODUCTION

The characterization of the potential energy functions between weakly interacting species has been the subject of extensive experimental and theoretical research.[1] The two-body and nonadditive forces that govern the interactions between these species provide a basis for understanding the long-range attractions between all atoms and molecules, as well as a microscopic picture of interatomic and intermolecular interactions in condensed phases. While much of the gas phase research has focused on interactions between closed-shell neutral molecules,[2] there has been considerable recent interest in the spectroscopy of weakly bound complexes involving open-shell atoms or molecules,[3] as well as positively and negatively charged clusters.[4]

Considerable progress has been achieved in characterizing the negatively charged clusters in recent years, using photoelectron spectroscopy,[5] infrared action spectroscopy,[6] and anion ZEKE (zero electron kinetic energy) photodetachment spectroscopy.[7] Photoelectron spectroscopy is the most general of these techniques, but its resolution of 5–10 meV is often insufficient to resolve low-frequency modes in clusters. IR spectroscopy can be applied when there is an appropriate infrared active chromophore in the complex, whereas anion ZEKE spectroscopy with its resolution of 1–2 cm^{-1} is particularly suited to anion complexes composed of weakly bound atomic moieties, in which case it directly probes the low-frequency vibrations characteristic of ion–neutral binding in the anion complexes and the weakly bound neutral species formed by photodetachment. Vibrationally resolved ZEKE spectra for selected diatomic[8–12] and polyatomic rare gas halide clusters (Rg_nX^-) have been reported.[13–15] Here we extend our investigations to the $XeCl^-$ anion.

Such studies of RgX^- diatomics provide accurate two-body potentials for the anionic and neutral species involved in the photodetachment process. The anion potentials are needed to understand the structure, energetics, and dynamics of larger halide clusters as well as the importance of nonadditive effects in species of this type.[13,14] Charged Rg_nX^- clusters are convenient model systems to study solvation at a microscopic level, and therefore help understanding of the photophysical properties and the reactivity of ions in the condensed phase. RgX^- interaction potentials also have important practical applications, as they are, e.g., needed to describe processes occurring in discharges and plasmas.

The only prior experimental information on the $XeCl^-$ anion comes from two sets of ion mobility measurements.[16,17] *Ab initio* calculations have been carried out at the CCSD(T) level of coupled cluster theory using a relativistic effective core potential (RECP) for Xe and an aug-cc-pVTZ basis set, including diffuse orbitals, for Cl^-.[18] High level *ab initio* calculations have also been carried out for the related $ArCl^-$ and $KrCl^-$ anions.[19] These data are complemented by potentials deduced from several theoretical and (semi-empirical models).[20–23] Thus, the ability to probe the anion in our ZEKE experiment is particularly valuable due to the absence of other spectroscopic information.

The neutral XeCl complexes accessed by photodetachment of the $XeCl^-$ anion are also of interest because of the open-shell nature of the chlorine atom. Three molecular electronic states result from the interaction between $Cl(^2P)$ and Xe.[24,25] The electrostatic interaction splits the lower $Cl(^2P_{3/2})$ state into two components that arise from two different projections of the total electronic angular momentum Ω along the Xe–Cl internuclear axis: $\Omega = \frac{1}{2}$ (the $X1/2$ state or X state) and $\Omega = \frac{3}{2}$ (the $I3/2$ or I state). The upper $^2P_{1/2}$ spin–orbit state of atomic chlorine correlates with a third state in the complex, $II1/2$ (the II state), characterized by $\Omega = \frac{1}{2}$.

Much of the original interest in neutral RgX species was due to their use in excimer lasers. Here lasing occurs through transitions between deeply bound charge transfer states (''Rg^+X^-'') and the weakly bound covalent ground states. XeCl was one of the first systems where such lasing action at 308 nm was reported.[26] For that reason there has been a great deal of interest to characterize the X, I, and II state potential

[a]Current address: Institut für Physikalische Chemie, Universität Göttingen, Tammannstraße 6, D-37077 Göttingen, Germany.
[b]Corresponding author. Fax: +01-510-642-3635; electronic mail: dan@radon.cchem.berkeley.edu

functions of XeCl. For example, emission spectra of the $X \leftarrow B$ and $X \leftarrow D$ transitions in $^{136}Xe^{35}Cl$ were recorded and analyzed by Tellinghuisen and co-workers, yielding spectroscopic constants for the X state.[27] Lee and co-workers performed differential cross section (DCS) measurements from which potential curves for the X, I, and II states were obtained.[28] More detailed information on these potentials came from absolute elastic total cross section (TCS) measurements with magnetic selection of the Cl atoms carried out by Aquilanti and co-workers.[29]

In the ZEKE experiments presented here we observe vibrationally resolved transitions to the X state of XeCl, but the $I \leftarrow$anion and $II \leftarrow$anion bands were undetectable, presumably due to extremely low s-wave partial detachment cross sections for these two neutral states. This was discussed in more detail in one of our earlier publications.[10]

This paper is organized as follows: in Sec. II we provide a short summary of the experimental setup. In Sec. III the $X \leftarrow$anion spectrum is presented and complete assignments of the observed transitions are given. In Sec. IV we briefly discuss the construction of model potentials for fitting the vibrational and rotational peak contours of the ZEKE spectrum. Finally, in Sec. V our $XeCl^-$ anion potential is confronted with the available literature data.

II. EXPERIMENT

The anion zero electron kinetic energy (ZEKE) spectrometer has been described in detail previously.[7,30] Briefly, $XeCl^-$ anions are formed by passing a mixture of 15% Xe and 85% He over CCl_4 at 0 °C, which is then expanded into a vacuum through a 0.5 mm aperture in a pulsed valve (General Valve Series 9). Typical backing pressures are 30–40 psig. The resulting free jet is crossed by a 1 keV electron beam. Dissociative attachment and other secondary processes produce negative ions, which subsequently undergo clustering in the continuum flow of the expansion. As the expansion progresses, the anion clusters formed during these processes are further cooled.

After passing through two skimmers, the anions enter a differentially pumped region where they are accelerated to 1 keV and then separate according to their mass in a 1 m colinear time-of-flight mass spectrometer. Photodetachment of the $XeCl^-$ anions in the following detector region is achieved by an excimer-pumped dye laser (Lambda Physik FL3002).

Approximately 400–500 ns after photodetachment, the electrons are extracted collinearly by a weak pulsed field of 4 V/cm and deflected to an off-axis MCP detector (Galileo) that is positioned about 1 m away from the extraction region. Gated electron detection assures temporal filtering of the photoelectrons, and a set of apertures between the photodetachment point and the detector provides spatial discrimination. This combination of spatial and temporal filtering yields efficient discrimination against high-energy electrons. Thus, when tuning the laser wavelength, only threshold photoelectrons with nearly zero kinetic energy are detected. As in our earlier work, a weak dc field of −15 mV/cm is maintained across the electron detachment region at all times,[10,14] which slightly decelerates electrons in the laboratory frame. This field enhances the ZEKE electron signal by roughly a factor of 3, with no loss of spectral resolution (1–2 cm^{-1}) for atomic anions.[10] The peaks observed in this study are broader due to unresolved rotational envelopes and hot band congestion.

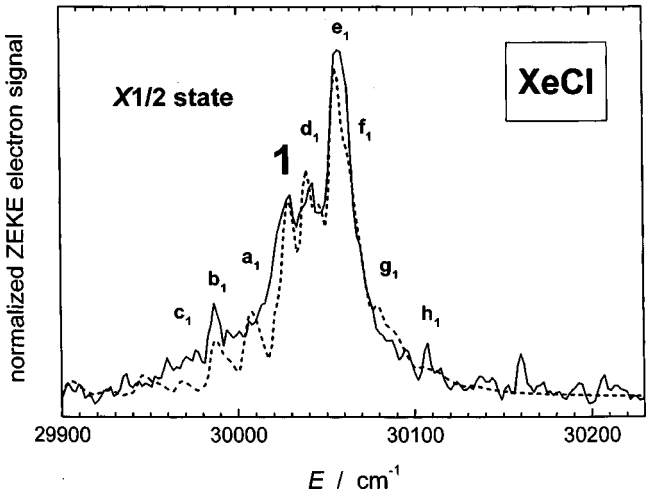

FIG. 1. The experimental and simulated $XeCl^-$ ZEKE spectrum for the $X1/2$ state [$Cl(^2P_{3/2}) + Xe$ asymptote]. Solid line: experimental data; dashed line: best fit spectral simulation based on the MMSV model potential for the anion and the ESMSV X state potential of Ref. 29. For complete assignments of peaks **1** and $a_1 - h_1$ see Table I.

The experiment is performed at a 30 Hz repetition rate. PTP dye (Exciton) is used with a typical energy of 3–15 mJ/pulse. The $XeCl^-$ ZEKE spectrum is normalized to the ion signal and laser power, and averaged over 3800 laser shots per point. Absolute vacuum wavelengths are obtained by calibration of the dye laser with a Fe/Ne hollow cathode lamp.

III. XeCl $X1/2$ STATE ZEKE SPECTRUM AND ASSIGNMENTS

Figure 1 shows the ZEKE spectrum for the transition from the anion to the $X1/2$ state (black line) together with an optimized spectral simulation (dashed line), obtained using the anion and neutral potentials described in Sec. IV. A list of peak positions and spectral assignments is given in Table I.

TABLE I. Peak assignments for the transitions between the $XeCl^-$ anion and the corresponding neutral $X1/2$ state (see also Fig. 1). All energies are in cm^{-1}. The assignment listed first contributes the most to the peak intensity. Assignments in parentheses are additional transitions needed to account for at least two-thirds of the total peak intensity.

Peak	Position	Relative energy	Assignment: $v'(X1/2) \leftarrow v''$ (anion)
1	30 029.6	0.0	3←2 (0←0)
a_1 (shoulder)	30 007.0	−16.6	4←3 (6←4)
b_1	29 988.2	−41.4	0←1 (5←4)
c_1	29 970.0	−59.6	6←5
d_1	30 042.4	+12.8	2←1 (4←2)
e_1	30 057.0	+27.4	1←0
f_1 (shoulder)	30 068.0	+38.4	3←1
g_1 (shoulder)	30 083.0	+53.4	2←0
h_1	30 107.5	+77.9	3←0

The vibrational frequency of the $XeCl^-$ anion is expected to be larger than that of the neutral XeCl $X1/2$ state. Different types of $X \leftarrow$ anion transitions in the spectrum can therefore be distinguished. First, there are vibrational progressions v'-0 in which a series of neutral vibrational levels v' is populated by transitions originating from the anion ground vibrational state $v''=0$. Transitions of this type to neutral levels with $v'>0$ occur at higher energies than the 0–0 transition. Second, there are v'-v'' transitions originating from excited anion levels: these can be further divided into sequence bands with *constant* Δv from a series of anion vibrational levels and single hot band transitions ($\Delta v \neq 0$).

The three most prominent features in the ZEKE spectrum are peaks e_1, **1**, and b_1, with e_1 being the most intense. In all other RgX^- ZEKE spectra we have reported,[8–11] the most intense band in the $X \leftarrow$ anion band was the 0–0 transition, suggesting an assignment of peaks e_1, **1**, and b_1 to the 0–0, 1–1, and 2–2 sequence band transitions, respectively. However, the three peaks should be equally spaced if this assignment were correct. Instead, peaks e_1 and **1** are spaced by 27 cm^{-1}, while peaks **1** and b_1 are spaced by 41 cm^{-1}. It is therefore more reasonable to assign peaks e_1, **1**, and b_1 to the 1–0, 0–0, and 0–1 transitions, yielding preliminary anion and neutral frequencies of 41 and 27 cm^{-1}, respectively. This assignment was used as a starting point in the simulations, which yield the more detailed assignments in Table I.

The simulation shows that peak **1** is due to several transitions: The main contributions arise from the 0–0 transition with about 30% and the 3–2 transition (from $v''=2$ in the anion to $v'=3$ in the $X1/2$ state) with roughly 40% of the total peak intensity. The latter transition together with the peaks e_1 and d_1, and the weaker features a_1, b_1, and c_1 form the ($\Delta v = v'$-$v''=1$) sequence band (1–0 to 6–5). The main contribution to peak b_1 is, however, due to the 0–1 transition. Peak e_1 and the weak shoulderlike features g_1 and h_1 belong to the (v'-0) progression in the $X1/2$ state with $v'=1-3$.

We did not observe any features for the *I* and *II* states of XeCl. From our experience with other rare gas halides this is expected, as it is found that the intensity of these bands (phenomenologically) decrease considerably with increasing size (polarizability) of the rare gas atom and decreasing diameter of the halide; e.g., in the XeI^- ZEKE spectrum the *I* state is barely visible,[10] and for $XeBr^-$ not observable.[9] This is probably due to pronounced differences in the *s*-wave partial detachment cross sections for the different neutral states, as discussed at length previously in our work[10] and in a recent theoretical study by Buchachenko *et al.*[19]

IV. ANALYSIS: POTENTIAL FUNCTIONS AND BEST FIT

From peak **1** in Fig. 1 we directly obtain an electron affinity of $30029.6 \pm 6.0\ cm^{-1}$ for $XeCl^-$. This value is larger than the corresponding electron affinity of atomic chlorine ($29\,138.59\ cm^{-1}$).[31] Therefore the dissociation energy of $XeCl^-$ is greater than that of XeCl, as expected. From the vibrational assignments in Table I, we can also deduce frequencies for the anion and the $X1/2$ state. For a more detailed description of the binding properties in the anion and the neutral, it is necessary to use a flexible model potential that can be used to simulate the ZEKE spectrum. The potentials, fitting procedure, and results are described below.

We cannot independently extract information on the equilibrium bond length of the anion and *X* state potentials because no rotational structure is resolved (experimental resolution $\geqslant 1\ cm^{-1}$). A similar situation occurs for the well depth ϵ, because we are only sensitive to the difference between the anion and *X* state. An external reference potential is therefore needed to determine the *absolute* position and well depth of the $XeCl^-$ anion potential curve. For this purpose we used the XeCl $X1/2$ state ESMSV (exponential-spline-Morse-spline-van der Waals) scattering potential from Aquilanti *et al.*[29] For the $XeCl^-$ anion potential we adopted a flexible piecewise Morse–Morse-switching function–van der Waals (MMSV) potential [with $f(x)=V(R)/\epsilon$ and $x=R/R_m$],

$$\begin{aligned} f(x) &= e^{2\beta_1(1-x)} - 2e^{\beta_1(1-x)}, \quad 0<x\leqslant 1, \\ &= e^{2\beta_2(1-x)} - 2e^{\beta_2(1-x)} \equiv M_2(x), \quad 1<x\leqslant x_1, \\ &= \mathrm{SW}(x)M_2(x) + [1-\mathrm{SW}(x)]W(x), \quad x_1<x<x_2, \\ &= -B_{4r}x^{-4} - B_{6r}x^{-6} \equiv W(x), \quad x_2\leqslant x<\infty, \end{aligned} \tag{1}$$

as used in our earlier work.[8–10,32] The switching function $\mathrm{SW}(x)$ is calculated via

$$\mathrm{SW}(x) = \frac{1}{2}\left(\cos\frac{\pi(x-x_1)}{(x_2-x_1)} + 1\right). \tag{2}$$

Here, ϵ is the potential well depth, and R_m represents the equilibrium bond length (position of the potential minimum). β_1 and β_2 are Morse parameters. B_{4r} denotes the coefficient of the leading term in the long-range $XeCl^-$ potential (reflecting the dipole induced on the xenon atom by the Cl^- anion), and B_{6r} consists of quadrupole induction and dipole dispersion terms. The latter two quantities can be calculated via

$$B_{4r} = \frac{B_4}{\epsilon R_m^4}, \quad B_{6r} = \frac{B_6}{\epsilon R_m^6}, \tag{3}$$

where B_4 and B_6 are given by

$$B_4 = \tfrac{1}{2}q^2\alpha_d(\mathrm{Xe}), \quad B_6 = \tfrac{1}{2}q^2\alpha_q(\mathrm{Xe}) + C_6. \tag{4}$$

Here, q is the chloride charge and $\alpha_d(\mathrm{Xe})$ and $\alpha_q(\mathrm{Xe})$ are the dipole and quadrupole polarizabilities of xenon, respectively [$\alpha_d(\mathrm{Xe}) = 27.16a_0^3, \alpha_q(\mathrm{Xe}) = 202.8a_0^5$].[33] The C_6 parameter of the $XeCl^-$ anion was taken from *ab initio* calculations ($C_6 = 299.49e^2a_0^5$).[34] The simulation of the ZEKE spectrum was not sensitive to the long-range part of the potential, so B_4 and B_6 were not changed during the fitting procedure.

As in our earlier studies, we used a discrete variable representation (DVR) procedure[35] based on a basis set of Morse potential eigenfunctions[36] to determine vibrational eigenvalues and wave functions for the anion and *X* state potential. Once this was done, Franck–Condon factors were calculated, assuming a Boltzmann distribution for the anion vibrational level population. From these a simulated vibra-

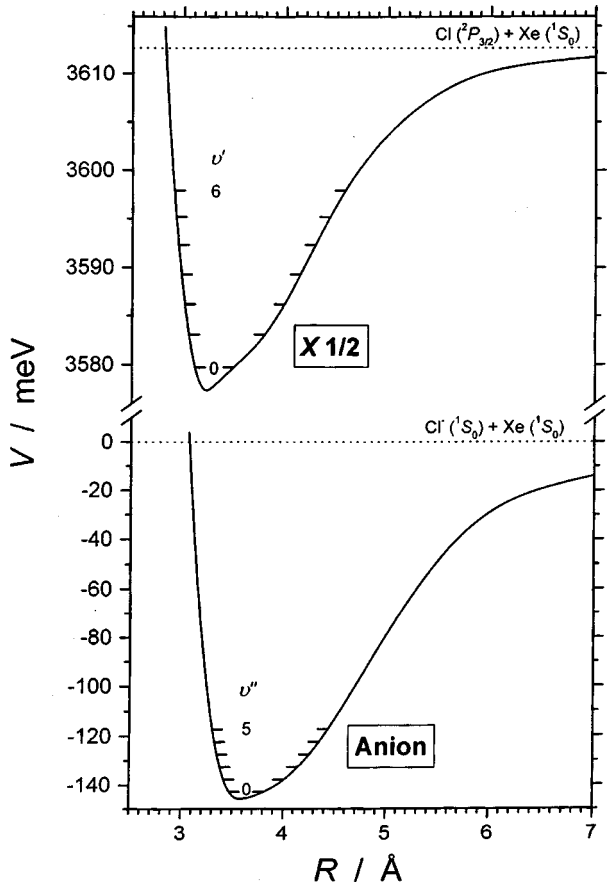

FIG. 2. The best fit MMSV model potential for the $XeCl^-$ anion and the neutral ESMSV $X1/2$ state potential of XeCl from Ref. 29. The anion asymptote for $R\rightarrow\infty$ is set to $E=0$, so the X state asymptotically converges toward the chlorine electron affinity (3612.726 meV) (Ref. 31). Note also the break on the energy axis. Vibrational states involved in transitions (Table I) contributing to observed features in the spectrum of Fig. 1 are marked by short dashes on the inner and outer potential wall of each state.

tional stick spectrum was produced. Finally, for each vibrational band a set of rotational lines was calculated, and these lines were convoluted with the ZEKE instrumental line shape to fit the observed asymmetric peak shapes. More details can be found in earlier publications.[8,9]

The well depth ϵ_{an} of the anion can be determined from the expression

$$\epsilon_{an}=\nu_{0-0}(X)+\omega_0^{an}+\epsilon_X-\omega_0^X-\mathrm{EA(Cl)}. \quad (5)$$

$\nu_{0-0}(X)$ represents the origin of the X state, ω_0^{an} and ω_0^X are the anion and X state zero-point energies, and EA(Cl) is the electron affinity of the chlorine atom. Once the well depth of the anion is fixed, the potential parameters R_m, β_1, β_2, x_1, and x_2 of the anion, the ZEKE linewidth, and the vibrational and rotational temperature of the anion were iteratively adjusted to reach the best agreement between the simulated and experimental ZEKE spectrum. From our spectral fits we deduced vibrational and rotational temperatures of $T_{vib}=190$ K and $T_{rot}=30$ K, respectively.

An optimized fit—especially with respect to the positions and intensities of peaks **1**, d_1 and e_1—was only possible for a very restricted set of parameters. The anion potential we obtain should therefore be quite accurate. We also tried to fit the weak irregular structure above 30 100 cm^{-1}, where transitions to the I state are expected. We carried out spectral simulations on the basis of the accurate $I3/2$ potentials of Aquilanti and co-workers[29] and our optimized anion potential. However, the peak at 30 160 cm^{-1} could not be fitted at all and the structures of even lower intensity only partly be reproduced. Thus, the features observed in this region are probably due to experimental noise.

TABLE II. MMSV potential parameters and deduced spectroscopic constants for the $XeCl^-$ anion. Term energy $T_0=30\,029.6$ cm^{-1} (see Fig. 1 and Table I) ω_0=zero-point energy, ν_{01}=fundamental vibrational frequency. Assumed anion temperature in the spectral simulation: $T_{vib}=190$ K and $T_{rot}=30$ K. Estimated fit uncertainties for potential parameters (±) are given in parentheses. The first number represents the uncertainty on the basis of the ZEKE fit, whereas the second number reflects a possible absolute shift due to uncertainties of the $X1/2$ reference ESMSV potential from scattering measurements.[29] The latter potential is characterized by $\epsilon=35.36$ meV, $R_m=3.23$ Å, $\omega_0=19.05$ cm^{-1}, and $\nu_{01}=27.05$ cm^{-1}.

ω_0 (cm^{-1})	23.26
ν_{01} (cm^{-1})	41.43
ϵ (meV)	145.82 (0.7,0.7)
R_m (Å)	3.57 (0.02,0.03)
β_1	4.90 (0.50)
β_2	2.30 (0.50)
x_1	1.05 (0.05)
x_2	1.80 (0.15)
B_4 (eV Å^4)	28.98 (4.35)
B_6 (eV Å^6)	239.54 (59.89)

In Fig. 2 the best fit anion potential is shown together with the $X1/2$ state potential from Aquilanti.[29] Note that the energy scale in the plot for the X state is magnified compared to the anion potential. The anion potential is about a factor of 4 deeper than the X state. The vibrational levels contributing to observed transitions in the spectrum of Fig. 1 have been marked by short dashes on the inner and outer potential wall and numbered (compare Table I). The locations of the turning points corresponding to the highest-energy levels contributing to spectral transitions allow us to estimate that the ZEKE $XeCl^-$ anion potential should be well defined over the interval $R=3.3$–4.4 Å, corresponding to roughly 20% of the classical potential well depth.

Table II shows the best fit parameters of the anion potential, including estimated uncertainties. The corresponding spectral simulation has already been included in Fig. 1 as a dashed line and discussed in Sec. III. Because the parameters B_4 and B_6 for the anion should be accurate to within ±15% to ±25%, the long-range behavior of our anion model potential should also be realistic. The $XeCl^-$ ZEKE spectrum is, however, not sensitive to the higher-energy region of the repulsive wall at short range. The anion potential can shift within the uncertainties of the reference values used for R_m and ϵ. These are also included in Table II.

V. DISCUSSION

We first consider the $XeCl^-$ anion potential obtained from our ZEKE experiments (Fig. 2 and Table II). The anion

TABLE III. A comparison of equilibrium bond lengths R_m and well depths ϵ for different rare gas halide clusters containing xenon or chlorine atoms.

		$ArCl^{(-)a}$	$KrCl^{(-)b}$	$XeCl^{(-)c}$	$XeBr^{(-)d}$	$XeI^{(-)e}$
R_m (Å)	anion	3.71	3.83	3.57	3.81	4.09
	$X1/2$	3.73	3.75	3.23	3.82	4.05
ϵ (meV)	anion	64.9	95.7	145.8	126.9	103.2
	$X1/2$	16.8	22.0	35.4	31.5	33.1

[a]Reference 11.
[b]Reference 9.
[c]This work (Table II).
[d]Reference 9.
[e]References 10 and 14.

TABLE IV. Characteristic quantities of the ZEKE $XeCl^-$ anion potential compared to literature potentials.

Source	ϵ (meV)	R_m (Å)
Present work[a]	145.8 (0.7)	3.57 (0.03)
Ion mobilities[b]	135	3.81
Ion mobilities[c]	198 (20)	3.30 (0.33)
Universal interaction potentials[d]	207	3.41
CCSD(T) (''BSI'' basis set)[e]	121 (43)	3.80
Unified perturbative approach[f]	187	3.47
Polarizability correlations[g]	148	3.97
Modified polarizability correlations[h]	138	3.87
Scaled electron gas approximation[i]	173	3.49
Surface potentials[j]	109	3.99

[a]Uncertainties in R_m and ϵ estimated from the $X1/2$ state reference potential of the scattering measurements from Ref. 29.
[b]Reference 16.
[c]Reference 17.
[d]Reference 39.
[e]Reference 18: relativistic effective core potential (RECP) for Xe, aug-cc-pVTZ basis set, including diffuse orbitals, for Cl^-.
[f]Reference 20.
[g]Reference 21.
[h]The same as (g), but using modified constants from Ref. 9.
[i]Reference 22.
[j]Reference 23.

well depth is about four times larger than that of the X state because of the much stronger attraction due to the leading charge-induced dipole term and the additional charge-induced quadrupole contribution in the anion [Eqs. (1), (3), and (4)]. The well depth of $XeCl^-$ is the deepest of all the rare gas chlorides, bromides, and iodides (see Table III), which confirms the observed trend that ϵ increases with increasing polarizability of the rare gas and decreasing size (= increasing charge density) of the halide anion.[8–11] Based on this trend and previous theoretical and experimental work,[18,21,37] we expect XeF^- to be even more strongly bound, but have not investigated it yet. Table III shows that R_m for $XeCl^-$ is smaller than for $XeBr^-$ or XeI^-, as expected, but it is also smaller than R_m for $ArCl^-$ and $KrCl^-$, implying that the bonding in $XeCl^-$ results in a significant distortion of the electron cloud around the Xe atom.

Photodetachment of $XeCl^-$ to the X state results in a decrease in R_m of 0.34 Å. As shown in Table III, this difference in bond lengths between the anion and X state is in marked contrast to the situation observed in all our earlier studies of other rare gas chlorides ($ArCl^-$,$KrCl^-$) and xenon halides ($XeBr^-$,XeI^-), for which the R_m values are, in general, very similar.[9–11,14] This result is immediately evident from the appearance of the ZEKE spectra. Whereas in the earlier studies the 0–0 transition dominates the X state spectrum as the highest peak, in the case of $XeCl^-$ its intensity is much lower the 1–0 transition (compare, e.g., peaks **1** and e_1 in Fig. 1). A closer inspection of Table III immediately shows that the equilibrium distance of the XeCl $X1/2$ state is by far the shortest of the neutral complexes. Following Aquilanti and co-workers, this can be explained by a strong stabilization of the Σ state due to configuration interaction with higher lying ionic (Xe^+Cl^-) molecular states of the same symmetry.[25,38]

Our ZEKE investigation yields the first reliable experimental well depth and geometry for the $XeCl^-$ anion. A comparison of ϵ and R_m with those from earlier studies is shown in Table IV. The only other experimental information comes from ion mobility measurements of two different groups,[16,17] which deviate considerably from each other and from the ZEKE results. Although it was shown by Viehland[17] that the potential of Thackston *et al.*[16] was obtained on the basis of an overly simplified data evaluation, the latter results nevertheless are closer to the ZEKE experiments than Viehland's potential.[17] Substantial deviations between ZEKE potentials and ion mobility data were also found for all the other systems studied so far.[8–10,14,37] It therefore appears as if an unambiguous inversion of ion mobilities into interaction potentials is not easily achievable. On the other hand, a recent study by Buchachenko *et al.*[40] indicates that the ZEKE potentials for the related ions $ArCl^-$ and $KrCl^-$ do not reproduce the ion mobility results, reflecting the fact that our experiments are insensitive to the repulsive, short-range interactions that govern the transport of ions in gases.

Table IV also shows $XeCl^-$ results from various semiempirical models and the *ab initio* calculation by Schröder *et al.*[18] All yield values of R_m and/or ϵ that are outside the uncertainty of our ZEKE potential. The ''unified perturbative approach'' [20] and the ''scaled electron gas approximation'' [22] both yield a too large well depth and a too short equilibrium bond length for $XeCl^-$. The ''polarizability correlations'' [21] and the CCSD(T) *ab initio* calculation[18] both result in too large values for R_m. We have used our ZEKE data on several other $RgX^{(-)}$ diatomics[8,9] to recalibrate the numerical coefficients in the polarizability correlation formulas.[21] When using these values the agreement for R_m becomes only slightly better.

Further improved models and theoretical calculations for a reliable representation of RgX^- anion potentials are clearly desirable. However, it also appears that some effort needs to be expended on developing potential energy functions that reproduce both the ZEKE spectra and ion mobility data.

VI. CONCLUSIONS

ZEKE spectroscopy of $XeCl^-$ was used to characterize the anion potential of this prototypical diatomic rare gas halide species. A simulation of the spectrum for the $X1/2$ state accessed by the photodetachment process allowed an assignment of all features. External experimental information on the neutral $X1/2$ state potential curve was necessary to deter-

mine the anion well depth and geometry. For this purpose, we used the X state ESMSV potential of Aquilanti and coworkers deduced from elastic total $Cl+Xe$ cross section measurements with magnetic state selection of the chlorine atom.[29] Due to the precision of this potential we estimate the uncertainties of the anion potential to be about ± 0.03 Å (R_m) and ± 0.7 meV (ϵ). We obtain the first accurate experimental potential for the $XeCl^-$ anion, which shows substantial differences in R_m and/or ϵ compared to earlier ion mobility measurements, semiempirical models, and *ab initio* data.

ACKNOWLEDGMENTS

This research is supported by the Air Force Office of Scientific Research under Grant No. F49620-00-1-0045. T.L. is grateful to the Deutsche Forschungsgemeinschaft for a postdoctoral fellowship, and M.R.F. thanks the National Science Foundation for a predoctoral fellowship.

[1] R. A. Aziz, in *Inert Gases*, edited by M. L. Klein (Springer-Verlag, Berlin, 1984), pp. 5–86; G. Chalasinski and M. M. Szczesniak, Chem. Rev. **94**, 1723 (1994).
[2] M. A. Suhm and D. J. Nesbitt, Chem. Soc. Rev. **24**, 45 (1995); K. Liu, J. D. Cruzan, and R. J. Saykally, Science **271**, 929 (1996).
[3] A. V. Komissarov and M. C. Heaven, J. Chem. Phys. **113**, 1775 (2000); M. I. Lester, B. V. Pond, M. D. Marshall, D. T. Anderson, L. B. Harding, and A. F. Wagner, Faraday Discuss. **118**, 373 (2001); M. Meuwly and J. M. Hutson, Phys. Chem. Chem. Phys. **2**, 441 (2000).
[4] A. W. Castleman, Jr. and K. H. Bowen, Jr., J. Phys. Chem. **100**, 12911 (1996).
[5] K. M. Ervin and W. C. Lineberger, in *Advances in Gas Phase Ion Chemistry* (JAI Press, Greenwich, 1992), Vol. 1, pp. 121–166.
[6] J. M. Lisy, Int. Rev. Phys. Chem. **16**, 267 (1997); J.-H. Choi, K. T. Kuwata, Y.-B. Cao, and M. Okumura, J. Phys. Chem. A **102**, 503 (1998); P. Ayotte, C. G. Bailey, G. H. Weddle, and M. A. Johnson, *ibid.* **102**, 3067 (1998).
[7] T. N. Kitsopoulos, I. M. Waller, J. G. Loeser, and D. M. Neumark, Chem. Phys. Lett. **159**, 300 (1989).
[8] Y. Zhao, I. Yourshaw, G. Reiser, C. C. Arnold, and D. M. Neumark, J. Chem. Phys. **101**, 6538 (1994).
[9] I. Yourshaw, T. Lenzer, G. Reiser, and D. M. Neumark, J. Chem. Phys. **109**, 5247 (1998).
[10] T. Lenzer, M. R. Furlanetto, K. R. Asmis, and D. M. Neumark, J. Chem. Phys. **109**, 10754 (1998).
[11] T. Lenzer, I. Yourshaw, M. R. Furlanetto, G. Reiser, and D. M. Neumark, J. Chem. Phys. **110**, 9578 (1999).
[12] V. Distelrath and U. Boesl, Faraday Discuss. **115**, 161 (2000).
[13] I. Yourshaw, Y. Zhao, and D. M. Neumark, J. Chem. Phys. **105**, 351 (1996).
[14] T. Lenzer, M. R. Furlanetto, N. L. Pivonka, and D. M. Neumark, J. Chem. Phys. **110**, 6714 (1999).
[15] T. Lenzer, I. Yourshaw, M. R. Furlanetto, N. L. Pivonka, and D. M. Neumark, J. Chem. Phys. **115**, 3578 (2001); N. L. Pivonka, T. Lenzer, M. R. Furlanetto, and D. M. Neumark, Chem. Phys. Lett. **334**, 24 (2001).
[16] M. G. Thackston, F. L. Eisele, W. M. Pope, H. W. Ellis, E. W. McDaniel, and I. R. Gatland, J. Chem. Phys. **73**, 3183 (1980).
[17] C. C. Kirkpatrick and L. A. Viehland, Chem. Phys. **98**, 221 (1985).
[18] D. Schröder, J. N. Harvey, M. Aschi, and H. Schwarz, J. Chem. Phys. **108**, 8446 (1998).
[19] A. A. Buchachenko, M. M. Szczesniak, and G. Chalasinski, J. Chem. Phys. **114**, 9929 (2001).
[20] S. H. Patil, J. Chem. Phys. **89**, 6357 (1988).
[21] D. Cappelletti, G. Liuti, and F. Pirani, Chem. Phys. Lett. **183**, 297 (1991).
[22] M. Waldman and R. G. Gordon, J. Chem. Phys. **71**, 1325 (1979).
[23] J. W. Wilson, J. H. Heinbockel, and R. A. Outlaw, J. Chem. Phys. **89**, 929 (1988).
[24] H. Haberland, Z. Phys. A **307**, 35 (1982).
[25] V. Aquilanti, D. Cappelletti, V. Lorent, E. Luzzatti, and F. Pirani, J. Phys. Chem. **97**, 2063 (1993).
[26] J. J. Ewing and C. A. Brau, Appl. Phys. Lett. **27**, 350 (1975).
[27] A. Sur, A. K. Hui, and J. Tellinghuisen, J. Mol. Spectrosc. **74**, 465 (1979).
[28] C. H. Becker, J. J. Valentini, P. Casavecchia, S. J. Sibener, and Y. T. Lee, Chem. Phys. Lett. **61**, 1 (1979).
[29] V. Aquilanti, D. Cappelletti, V. Lorent, E. Luzzatti, and F. Pirani, Chem. Phys. Lett. **192**, 153 (1992).
[30] C. C. Arnold, Y. Zhao, T. N. Kitsopoulos, and D. M. Neumark, J. Chem. Phys. **97**, 6121 (1992).
[31] U. Berzinsh, M. Gustafsson, D. Hanstorp, A. Klinkmüller, U. Ljungblad, and A.-M. Martensson-Pendrill, Phys. Rev. A **51**, 231 (1995).
[32] P. Casavecchia, G. He, R. K. Sparks, and Y. T. Lee, J. Chem. Phys. **77**, 1878 (1982).
[33] A. Kumar and W. J. Meath, Mol. Phys. **54**, 823 (1985); C. Hattig and B. A. Hess, J. Phys. Chem. **100**, 6243 (1996).
[34] C. Hattig and B. A. Hess, J. Chem. Phys. **108**, 3863 (1998).
[35] J. C. Light, I. P. Hamilton, and J. V. Lill, J. Chem. Phys. **82**, 1400 (1985).
[36] E. M. Greenawalt and A. S. Dickinson, J. Mol. Spectrosc. **30**, 427 (1969).
[37] L. A. Viehland and C. C. Kirkpatrick, Chem. Phys. **202**, 285 (1996).
[38] V. Aquilanti, D. Cappelletti, and F. Pirani, Chem. Phys. Lett. **271**, 216 (1997).
[39] A. D. Koutselos, E. A. Mason, and L. A. Viehland, J. Chem. Phys. **93**, 7125 (1990).
[40] A. A. Buchachenko, R. V. Krems, M. M. Szczesniak, Y. D. Xiao, L. A. Viehland, and G. Chalasinski, J. Chem. Phys. **114**, 9919 (2001).